A highly ionic conductive succinonitrile-based composite solid electrolyte for lithium metal batteries

Genrui Qiu[1,2], Yapeng Shi[1,2], and Bolong Huang[1,2,3] (✉)

[1] CAS Center for Excellence in Nanoscience, Beijing Institute of Nanoenergy and Nanosystems, Chinese Academy of Sciences, Beijing 100083, China
[2] School of Nanoscience and Technology, University of Chinese Academy of Sciences, Beijing 100049, China
[3] Department of Applied Biology and Chemical Technology, The Hong Kong Polytechnic University, Hung Hom, Kowloon, Hong Kong 999077, China

ABSTRACT

Solid-state Li metal batteries with solid electrolytes have built a potential way to solve the safety and low energy density problems of current commercial Li-ion batteries with liquid electrolyte. As a key component of solid-state Li metal batteries, solid electrolytes require high ionic conductivities and good mechanical properties. We have designed a composite solid electrolyte (CSE) consisting of poly(vinylidene fluoride-hexafluoropropylene) (PVDF-HFP)-$Li_{6.5}La_3Zr_{1.5}Ta_{0.5}O_{12}$ (LLZTO)-succinonitrile (SN) and Li bis(trifluoromethylsulphonyl)imide (LiTFSI). The PVDF-HFP-based porous matrix made by electrospinning ensures good mechanical properties of the electrolyte membrane, and the large proportion of SN filling material makes the electrolyte membrane have an ionic conductivity of 1.11 mS·cm^{-1} without the addition of liquid electrolyte. The symmetric battery assembled with CSE can be cycled stably for more than 600 h, and the $LiFePO_4$|CSE|Li full battery can also be cycled stably for more than 200 cycles. In addition to Li metal batteries, $Li-O_2$ and $Li-CO_2$ batteries that use CSE as electrolytes also have good performances, reflecting the universality of CSE. CSE does not only guarantee good mechanical properties but also obtain a high ionic conductivity. This design provides a new idea for the commercial application of polymer-based solid batteries.

KEYWORDS

Li metal batteries, composite solid-state electrolyte, succinonitrile, ionic conductivity, mechanical strength

1 Introduction

Energy shortage and environmental pollution have become urgent problems for mankind with the rapid development of society. Therefore, changing the energy structure, developing renewable energies such as wind, solar, and ocean energy, and increasing the proportion of clean energies are of great significance for solving the energy crisis and reducing pollutants. The randomness and periodicity of the above-mentioned clean energies require us to develop efficient energy storage devices [1]. As a new type of energy storage device that has received abroad attention, Li batteries have been widely used in portable electronic products, electric vehicles and aerospace, and other fields because of their high specific energy, long service life, low environmental pollution, and low self-discharge rate [2, 3]. Meanwhile, safety and higher energy density are the challenges faced by Li batteries, therefore solid-state Li batteries were invented to solve the above problems [4]. The application of solid electrolytes can effectively suppress the growth of Li dendrites, thereby reducing the safety risks caused by battery short-circuits [5]. In addition, solid electrolytes make it possible to apply Li metal negative electrodes, generating Li batteries with a higher energy density.

The solid electrolytes under studying are mainly divided into three types: (1) Inorganic solid electrolyte with high ionic conductivity and ion mobility at room temperature has high mechanical strength and wide operating temperature range. However, good mechanical strength also leads to poor interfacial contact and high interfacial resistance between the electrolyte and electrodes. Some electrolyte materials are prone to occur side reactions with Li, which also limits the service life and application range of the electrolytes. In addition, high cost is also a difficulty faced by the practical application of inorganic ceramic electrolytes [6]. (2) Polymer solid electrolyte with good interface contact is low cost and easy processing. However, the ionic conductivity at room temperature is much lower than that of liquid electrolytes and even inorganic solid electrolytes, which is a problem that polymer electrolytes must be solved [7]. (3) Composite solid electrolytes (CSEs), mainly dividing into polymer-based and ceramic-based CSEs, combine the advantages of the above two to a certain extent, but the improved ionic conductivity still does not meet the requirements of commercialization [8]. To advance the practical application of polymer-based solid electrolytes, improving the ionic conductivity at room temperature is an unignorable problem.

Because the transport of Li ion in the polymer-based solid electrolytes is mainly realized by the migration of the organic segments in the amorphous region, improving the ion conductivity requires increasing the number of free segments in the polymer collective or improving their mobility [9, 10]. Adding Li$^+$ conductors, such as $Li_7La_3Zr_2O_{12}$ (LLZO), $Li_{1+x}Al_xTi_{2-x}(PO_4)_3$ (LATP), etc., to the CSEs can reduce the crystallinity of the polymer and increase the number of Li ions, thereby increasing the ion conductivity [11–13]. Compared with LLZO, the addition

Address correspondence to bhuang@polyu.edu.hk

of Ta can increase the Li vacancies in the ceramic material so that $Li_{6.5}La_3Zr_{1.5}Ta_{0.5}O_{12}$ (LLZTO) has higher ionic conductivity. Meanwhile, unlike LATP that can be reduced by metal Li anode, LLZTO has no side reaction with Li, which is more suitable as an inorganic ceramic additive [5]. The polymer matrix is prepared by blending two or more organic substances, such as poly(ethylene oxide) (PEO), polyacrylonitrile (PAN), polyvinylidene fluoride (PVDF), etc., can also reduce the crystallinity of the polymer, and combines the advantages of multiple polymers [14–16]. It is also possible to increase the number of active segments by adding some polymers with higher segment activity, such as polysiloxane-based polymers and polycarbonate-based polymers [17–19]. Plastic crystals, such as succinonitrile (SN), etc., are also often used as additives to increase the ionic conductivity of the polymer [17, 20–22], because a small amount of SN can reduce the crystallinity of the polymer, and be a carrier for the migration of Li ions. But a large amount of SN will reduce the length of the organic chain segment and the mechanical strength of the polymer, not beneficial for suppressing the growth of Li dendrites.

In this work, we produced a CSE. The poly(vinylidene fluoride-hexafluoropropylene) (PVDF-HFP)-LLZTO porous matrix made by electrospinning ensures the good mechanical properties of the electrolyte membrane. And the large proportion of SN pouring material makes the electrolyte membrane have up to 1.11 mS·cm^{-1} ions conductivity at room temperature without the addition of liquid electrolyte, much higher than the commonly used polymer-based solid electrolytes. The symmetric battery assembled with CSE can be cycled stably for more than 600 h, and the full battery can also be cycled stably for more than 200 cycles. In addition, CSE can also be used as an electrolyte in Li-O$_2$ and Li-CO$_2$ batteries. This work provides guidance for the development of commercial polymer-based solid electrolytes with ultra-high ionic conductivity and good mechanical properties.

2 Experimental section

2.1 Preparation of PVDF-HFP/LLZTO electrospinning film

1 mL dimethylacetamide (DMAC) and 2 mL acetone (CH$_3$COCH$_3$) were mixed to obtain a solvent, then 0.5 g PVDF-HFP was added thereto and stirred until dissolved. Next, 0.1 g LLZTO powder was added to the above solution, the mixture was sonicated for 30 min, and then stirred at room temperature for 12 h. The prepared solution was immitted into the syringe for electrospinning. The obtained film was dried in a vacuum oven at 70 °C for 12 h to obtain PVDF-HFP/LLZTO electrospinning film. The synthesis method of LLZTO refers to our previous work [23].

2.2 Preparation of PVDF-HFP/SN/Li bis(trifluoro-methylsulphonyl)imide (LiTFSI) casting film

0.5 g PVDF-HFP was added to 3 mL dimethyl sulfoxide (DMSO), being stirred at 60 °C until the solid was dissolved. Then 0.5 g of SN and 0.2 g of LiTFSI were added to the solution in sequence, and the mixture was stirred for 12 h at 60 °C to obtain the precursor solution. The obtained precursor solution was poured onto a glass plate and dried at 30 °C for 5 h, and then dried in vacuum at 50 °C for 24 h to obtain PVDF-HFP/SN/LiTFSI casting film.

2.3 Preparation of CSE membrane

The obtained PVDF-HFP/LLZTO electrospinning film was fixed on a glass plate, and the precursor solution for making the PVDF-HFP/SN/LiTFSI casting film was evenly poured on the electrospinning film using a spatula at a height of 100 μm, next they were dried at 30 °C for 5 h, and then dried in vacuum at 50 °C for 24 h to obtain CSE membrane. Then the CSE was punched into discs with a diameter of 16 mm for use.

2.4 Characterization of CSE membrane

The surface structure of CSE was characterized by field emission scanning electron microscope (FE-SEM, SU8020). An electronic universal testing machine (INSTRON 5982) was used to test the mechanical properties of the electrolyte membrane at a stretching rate of 1 mm·min^{-1}. The functional groups of CSE were studied by Fourier transform infrared spectroscopy (FTIR, Perkin Elmer Frontier in ATR mode) in the 600–4,000 wavenumber range. Thermogravimetric analysis (TGA, SDT Q600 V20.9 Build 20) was used to study the thermal stability of the CSE membrane. The test was raised from room temperature to 600 °C in a N$_2$ atmosphere with a heating rate of 5 °C·min^{-1}. The electrochemical performance test refers to our previous work [23].

2.5 Preparation of Li-O$_2$ and Li-CO$_2$ batteries

0.06 g of C black, 0.03 g of commercial RuO$_2$, and 0.01 g of PVDF were added to 3 mL of N-methyl pyrrolidone (NMP) solvent and stirred uniformly to obtain a catalyst suspension. The suspension was evenly coated on C cloth and dried in vacuum to obtain a positive electrode. Then the Li chip, CSE, and positive electrode were assembled in a glove box with a battery case with holes to obtain Li-O$_2$ and Li-CO$_2$ batteries according to the previous method [23].

3 Results and discussion

In order to improve the ionic conductivity of the electrolyte membrane without reducing the mechanical strength, we chose the electrospinning membrane as the support, combined with the high ionic conductivity pouring material, to obtain a CSE. As shown in Fig. 1(a), PVDF-HFP with the added LLZTO was made into a porous film by electrospinning [24]. Pure-phase LLZTO (Fig. S1 in the Electronic Supplementary Material (ESM)) mixed into PVDF-HFP could not only replace inorganic fillers, but also produce a synergistic effect with polymers, which was beneficial to the ion transport of the film. The PVDF-HFP and SN mixed solution added with LITFSI was poured on the porous film, and after drying a mixed solid electrolyte film with high ionic conductivity and good mechanical strength was obtained. The high ionic conductivity of the CSE is due to the addition of plastic crystal SN. The addition of SN blocks the crystallization of PVDF-HFP, which increases the number of free segments [25, 26]. The conduction of Li ions in the polymer depends on the movement of the free segments [27]. At the same time, SN can also be used as a carrier for ion migration [28]. Therefore, the ionic conductivity of the CSE is relatively high. The CSE combined the advantages of the two electrolyte membranes in line with our design as shown in Fig. S2(a) in the ESM. The PVDF-HFP-based electrospinning film is used as the support to obtain higher mechanical strength. At the same time, the PVDF-HFP/SN-based electrolyte is used as the filler playing a role in improving ion conductivity. Figures 1(b) and 1(c) show the micromorphology of the CSE film. Comparing with Fig. S2(b) in the ESM, Fig. 1(b) proves that the perfused PVDF-HFP/SN completely wrapped and connected the filaments on the entire surface of the electrospinning film. Therefore, the high-conductivity electrolyte contacted with the electrode more uniformly and comprehensively. From Fig. 1(c) and Fig. S2(c) in the ESM, we find that the upper and lower filaments inside the electrospinning film were also connected by the perfused PVDF-HFP/SN. The above evidence shows that the ion conduction of the film mainly depended on the high ion conductivity part.
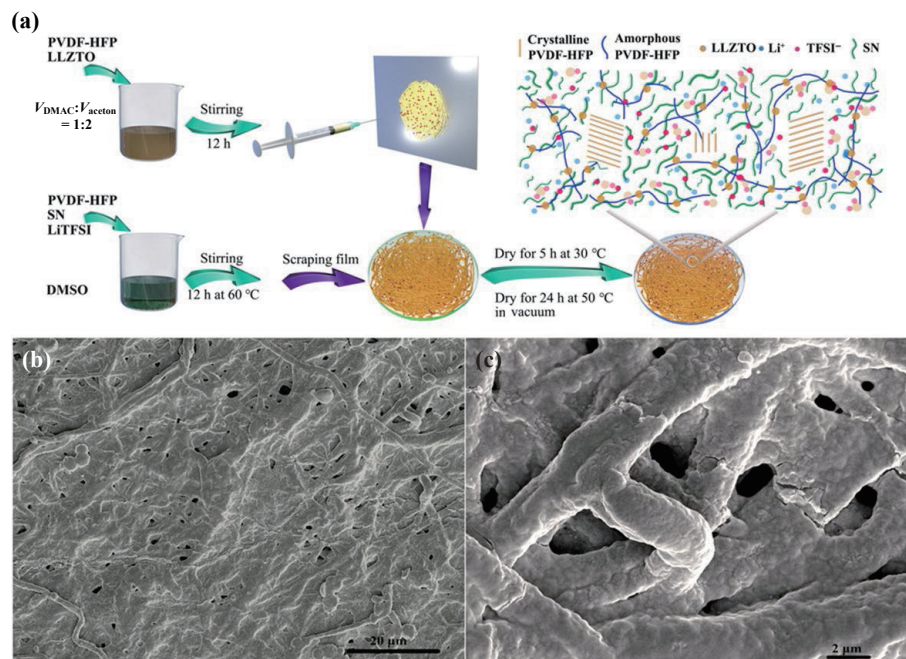
Figure 1 (a) Schematic diagram of preparing CSEs and the mechanism of adding SN to reduce the crystallinity of PVDF-HFP and thereby increase the ionic conductivity. (b) and (c) SEM images of the CSE membrane.

In order to determine the composition of the poured polymer, PVDF-HFP/SN/LiTFSI mixtures with different SN contents were cast on the glass plate to form a film and the ionic conductivity was tested. As shown in Fig. S3 in the ESM, the ionic conductivities at room temperature calculated by the Nyquist impedance spectra are 0.04, 0.09, 0.2, 0.56, 0.92, and 2.17 mS·cm⁻¹, corresponding to the wt.% of SN: 0%, 10%, 20%, 30%, 40%, and 50%, respectively. Summarizing them in Fig. 2(a), the ionic conductivity of the membrane increases almost exponentially as the SN content increases, proving that the addition of SN plays a determining role in the increase of ion conductivity. However, as shown in Fig. S4 in the ESM, the electrolyte membrane is so soft that can be torn gently when the wt.% of SN achieves 50%. Even when the wt.% of SN exceeds 50%, the polymer is difficult to obtain a complete film. Therefore, PVDF-HFP/SN/LiTFSI mixtures in which the wt.% of SN is 50% are selected as castable to prepare CSE film.

Figure 2(b) shows the Nyquist impedance spectra of CSE, from which the ionic conductivity of CSE at room temperature is calculated to reach 1.11 mS·cm⁻¹. The ionic conductivity of CSE is higher than the one without SN (4.63×10^{-5} mS·cm⁻¹) as shown in Fig. S5 in the ESM, proving that the addition of a high proportion of SN does greatly improve the ionic conductivity. More than that, the ionic conductivity of CSE is higher than that of most polymer solid electrolytes as shown in Table S1 in the ESM, which proves the huge advantage of CSE in ionic conductivity [7]. In addition, the Nyquist impedance spectra of CSE at different temperatures are tested as shown in Fig. 2(c) to further study the electrochemical properties of CSE. As the temperature increases, the resistance of CSE gradually decreases, but the decreasing amplitude is different around 60 °C, which proves that a factor affecting ion conductivity has changed around 60 °C. Furthermore, according to the data in Fig. 2(c), an Arrhenius plot as shown in Fig. 2(d) is drawn to calculate the activation energy (E_a) of CSE. The turning point of the Arrhenius plot corresponds to the melting point temperature of SN (54–56 °C), which proves
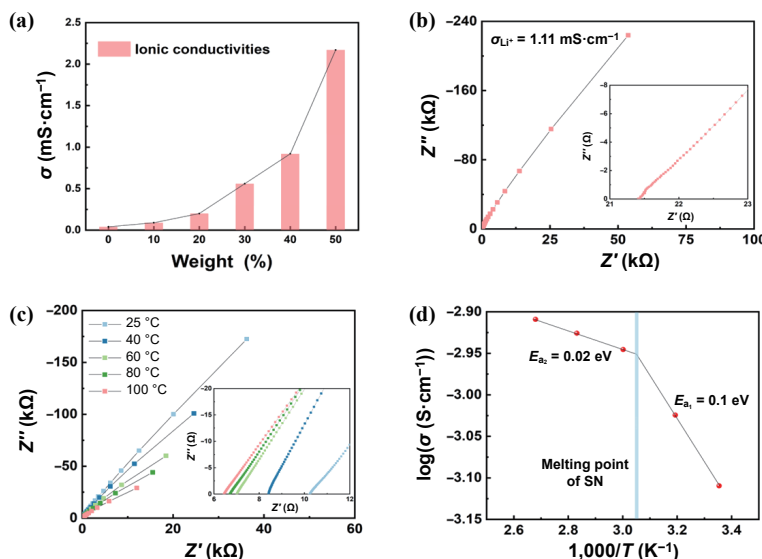

Figure 2 (a) Ionic conductivities of PVDF-HFP/SN/LiTFSI casting films varying with SN content at room temperature. (b) Nyquist impedance spectra of the CSE film at room temperature. (c) Nyquist impedance spectra of the CSE film at different temperatures. (d) Arrhenius plot of the CSE film.

that SN does not only play a role in reducing the crystallinity of the polymer, but also directly participate in the transport process of Li ions as a carrier of Li ions. When the temperature is below 60 °C, the E_a of the CSE is 0.1 eV, which is lower than most polymer-based solid electrolytes but close to gel electrolytes [24, 29–31]. This also explains the high ionic conductivity of CSE. When the temperature is higher, the E_a is greatly reduced to 0.02 eV, because SN changes from solid to liquid at this time, and the ion transport capacity of CSE is improved. As we designed, the addition of SN makes CSE have excellent electrochemical performance.

CSE does not only have high ionic conductivity, but also have outstanding electrochemical performance. As shown in Fig. 3(a), the Li-ion migration number (t_{Li^+}) of CSE is measured by chronoamperometry combined with electrochemical alternating current (AC) impedance method. The resistance of the Li|CSE|Li battery before polarization is 613 Ω, and the resistance after polarization reaches 578 Ω (the equivalent circuit diagram is shown in Fig. S6 in the ESM). The initial current before polarization is 13.98 μA, and the stable current after polarization is 13.04 μA. The calculated t_{Li^+} of CSE is 0.54, which is higher than 0.3–0.4 of commercial liquid electrolytes [32]. A high t_{Li^+} means that CSE has a high Li ions transmission efficiency. Combined with the high ion conductivity of CSE, it proves that CSE has an excellent Li ions transport capacity. In addition, the excellent electrochemical stability of CSE can also be demonstrated through the electrochemical window measured by linear sweep voltammetry (LSV) shown in Fig. 3(b). The electrochemical

window of CSE is as high as 4.7 V, which is much higher than that of liquid electrolyte, and can match most current high-voltage cathode materials.

CSE does not only have a good electrochemical performance, but also have a high mechanical performance as shown in Fig. 3(c). The tensile strength and elongation of CSE (10.7 MPa and 249%) are better than PVDF-HFP/LLZTO electrospinning films (6.2 MPa and 123%). This also proves that the infused PVDF-HFP/SN connects the spinning, making the mechanical properties of CSE not only stronger than the PVDF-HFP/SN/LiTFSI casting film, but also stronger than the PVDF-HFP/LLZTO electrospinning film. Combination of spinning porous support and high ionic conductivity pouring material makes CSE have higher mechanical strength to inhibit the growth of Li dendrites. We demonstrate the good thermal stability of CSE by its TGA thermogram in Fig. 3(d). Generally, the temperature at which the weight loss reaches 95% is considered as the starting temperature of thermal degradation [33]. When the temperature is higher than 98 °C, the CSE loses weight to 95%, which is due to the sublimation of SN, and only the evaporation of residual solvent occurred before that. To sum up, it can be considered that the thermal stability of CSE reaches 98 °C, which is much better than the current commercial liquid electrolyte [34]. We use FTIR to detect the functional groups presented in CSE and determine the presence of SN (Fig. 3(e)). The characteristic absorption peaks of PVDF-HFP as the main material are shown at 1,401 cm^{-1} (–C–F stretch peak) and 1,174 cm^{-1} (–CF$_2$– stretch peak). The vibration peak of the C–C skeleton at 1,074 cm^{-1}, the vinyl peak at 877 cm^{-1},
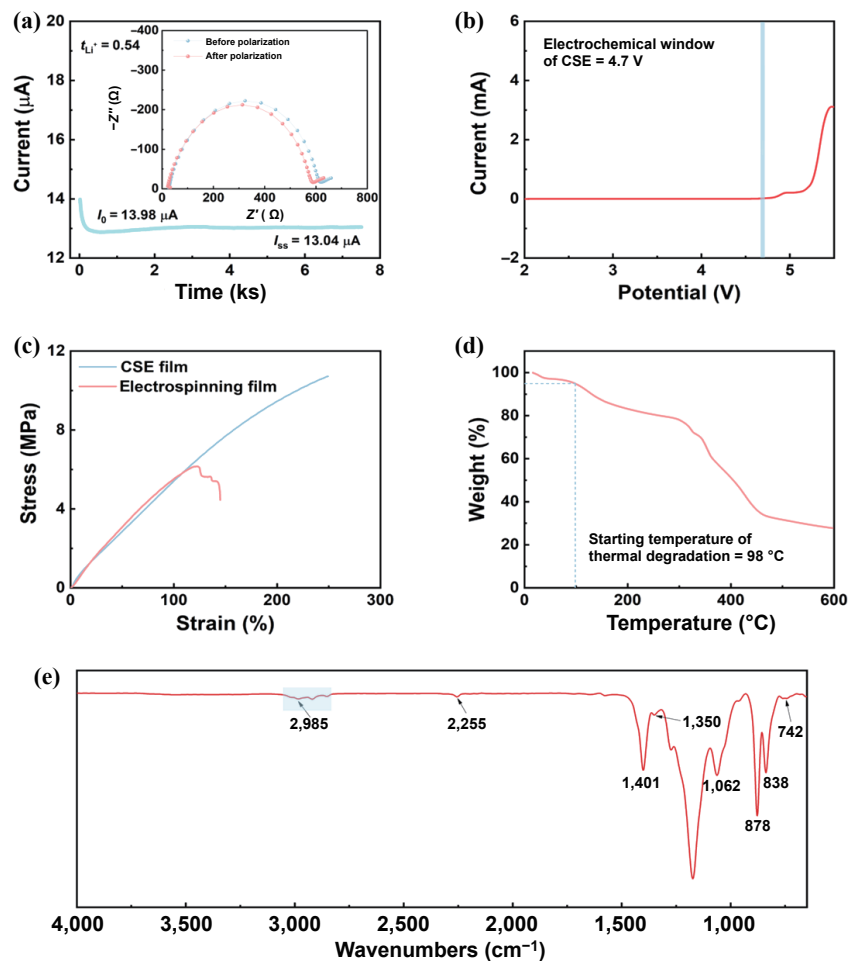

Figure 3 (a) Current–time profile of a symmetrical Li|CSE|Li cell after applying a direct current (DC) voltage of 10 mV on the cell, used for determining Li$^+$ transfer number. The insets show the Nyquist impedance spectra of the cell before and after polarization. (b) LSV image of the CSE film. (c) Stress–strain curves of the CSE and PVDF-HFP/LLZTO electrospinning film. (d) TGA thermogram of the CSE film. (e) FTIR spectrum of the CSE film.

and the CF$_3$ stretching peak at 835 cm^{-1} are also attributed to PVDF-HFP [35–37]. The small peaks at 1,350 and 742 cm^{-1} correspond to the lower content of TFSI$^-$ [28, 36, 38]. Several peaks related to SN appear at 2,985 cm^{-1}, and the peak at 2,255 cm^{-1} corresponding to C≡N is also attributed to SN [28], which also shows that SN exists in CSE in a free state and does not react with other organic substances, which confirms our inference above.

CSE possessing high ionic conductivity and high mechanical strength is used to assemble Li|CSE|Li symmetrical batteries and LiFePO$_4$|CSE|Li full batteries to verify the compatibility of CSE with positive and negative electrodes and electrochemical performance. In order to optimize the contact between the solid electrolyte and the electrodes, we dropped 8 μL of commercial electrolyte (1M LiPF$_6$ in EC:DEC:EMC = 1:1:1) on both sides of the solid electrolyte when assembling symmetrical and full batteries. As shown in Fig. 4(a), the Li|CSE|Li symmetrical battery can be cycled stably for 600 h at a current density of 0.2 mA·cm^{-2}, and the polarization voltage during the cycle is lower than 50 mV,

proving the high ionic conductivity and cycle stability of CSE. Moreover, it can be seen from the partially enlarged view that during the Li deposition/stripping process, the voltage plateau keeps stable and the polarization voltage does not increase nearly, indicating that the interface between CSE and Li metal is stable and no side reactions occur. When the current density is 0.4 mA·cm^{-2}, the Li|CSE|Li symmetrical battery can be cycled stably for 400 h with a slight increase in polarization voltage (Fig. S7 in the ESM). Figure 4(b) shows the charge and discharge curves of the LiFePO$_4$|CSE|Li full battery at different rates. The voltage curve keeps smooth and stable during the charging and discharging process, which proves that the battery has no side reactions. As the charge and discharge rate increases, the battery capacity decreases slightly, and the polarization voltage increases tinily. When the charge–discharge rate is 1 C, the reversible specific capacity of the battery reaches 156.7 mAh·g^{-1}, and when the rate is 2 C, the reversible specific capacity can still reach 148.8 mAh·g^{-1}. The battery can still maintain a high reversible charge–discharge specific capacity at a high charge–discharge rate.
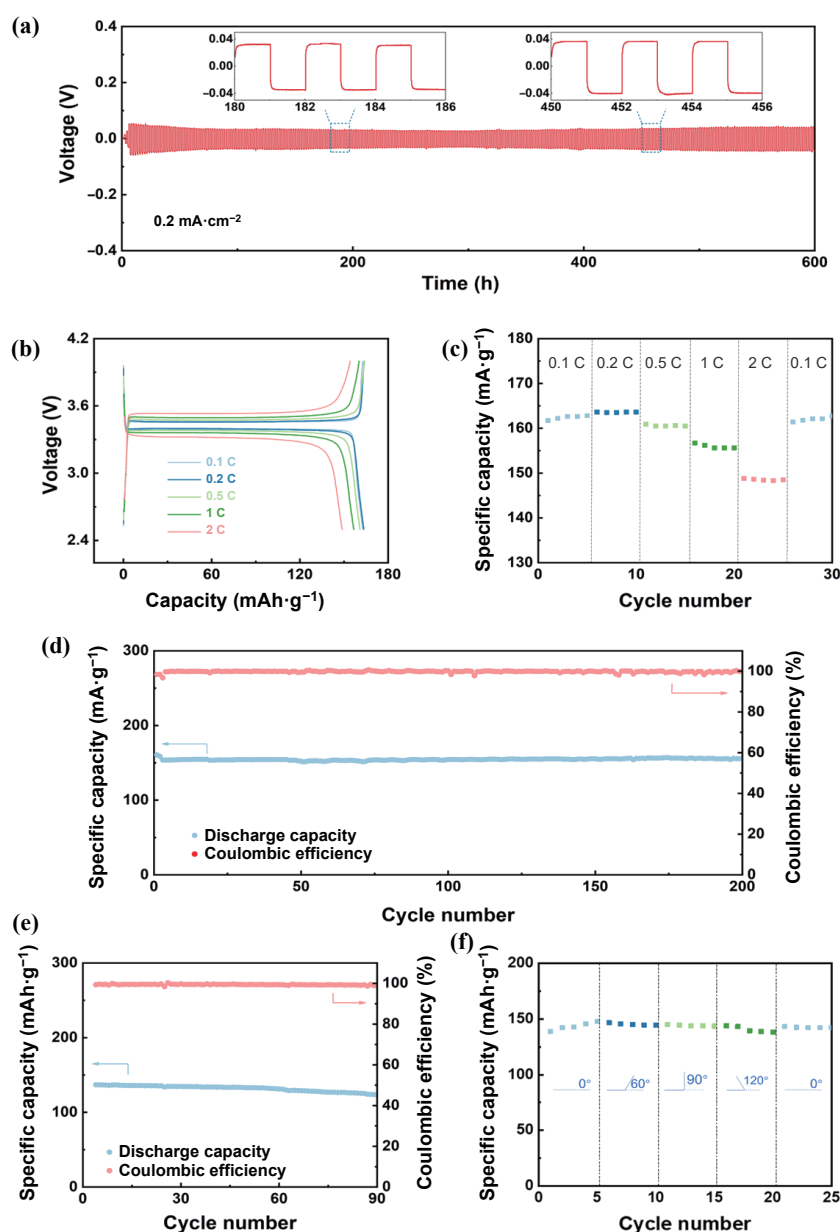

Figure 4 (a) Voltage distribution of the symmetrical Li|CSE|Li cell during cycling at a current density of 0.2 mA·cm^{-2} at room temperature. (b) The charge and discharge curves of the LiFePO$_4$|CSE|Li battery at different rates at room temperature. (c) The rate performance of the LiFePO$_4$|CSE|Li battery at room temperature. (d) The long-term cycle performance of the LiFePO$_4$|CSE|Li battery at a rate of 0.5 C at room temperature. (e) Long-term cycle performance of the flexible LiFePO$_4$|CSE|Li battery at 0.5 C rate at room temperature. (f) Cycle performance of the flexible battery with different bending angles at room temperature.

In order to further demonstrate the extraordinary rate performance of CSE, the capacity of the full battery at a different rate is shown in Fig. 4(c). After the battery has been charged and discharged for 5 times at different rates, the specific capacity of the battery can still be restored to the initial level after the charge–discharge rate is restored to 0.1 C, indicating that the interior of the battery has not been irreversibly damaged during the process of charging and discharging at high rates, and further explaining the good rate performance of the CSE. In addition to excellent rate performance, CSE also has good cycle stability. As shown in Fig. 4(d), after 300 cycles of stable cycling at 0.5 C, the Coulombic efficiency (CE) of the full battery still reaches 99%, and the specific capacity reaches 146.7 mAh·g⁻¹, which is 98% of the initial specific capacity, and the full battery can be cycled stably for 100 cycles even at 1 C (Fig. S8 in the ESM). In addition to its excellent electrochemical performance, CSE has another advantage that it can be used to make flexible solid-state batteries. Figure S9 in the ESM shows the process of lighting up the watch with a flexible LiFePO$_4$|CSE|Li battery. The flexible battery can be stably cycled for more than 90 cycles as shown in Fig. 4(e). Even in the case of bending, the flexible battery can still work normally. Figure 4(f) shows that when the flexible battery is bent at 0°, 60°, 90°, and 120°, the specific capacity of the battery fluctuates very little. When it returns to 0°, the flexible battery can still return to normal working conditions. The flexibility of CSE allows it to be applied to soft-pack batteries and to supply power for flexible electronic devices, which will greatly increase its wide range of applications.

Further displaying the wide applicability of CSE, it is used as an electrolyte in Li-O$_2$ and Li-CO$_2$ batteries using commercial RuO$_2$ as catalyst. At current densities of 100–500 mA·g⁻¹ with a limited capacity of 1,000 mAh·g⁻¹, the charging and discharging curves of Li-O$_2$ cell are shown in Fig. 5(a). As the current density gradually increases from 100 to 500 mA·g⁻¹, the charging platform increases slightly. When the current density is 500 mA·g⁻¹, the battery can still be fully charged within 4.5 V after discharge. Selecting 400 mA·g⁻¹ as the current density of the cycle test, when the limited capacity is 500 mAh·g⁻¹ and the voltage range is 2–4.5 V, the Li-O$_2$ battery can run stably for 62 cycles (Fig. S10(a) in the ESM), which is not inferior to liquid Li-O$_2$ batteries [39]. In Fig. 5(b), the charging and discharging platforms during the cycle are shown. The discharge platform of the battery changes very little during cycling, and the polarization voltage only increases slightly. In addition, the same catalyst and CSE are also used to assemble Li-CO$_2$ batteries. Similarly, the charge–discharge curves at current densities of 100–400 mA·g⁻¹ prove the good rate performance of the Li-CO$_2$ cell using CSE (Fig. 5(c)). As shown in Fig. 5(d) and Fig. S10(b) in the ESM, the Li-CO$_2$ battery applied with CSE can be cycled stably for 34 cycles at a current density of 200 mA·g⁻¹ and with a limited capacity of 500 mAh·g⁻¹, with discharge voltage having almost no decrease. Compared with the liquid battery using the same catalyst, the life of Li-CO$_2$ battery with CSE is close, which demonstrates the excellent electrochemical performance of CSE [40–42]. It shows that CSE can be well applied to Li-O$_2$ and Li-CO$_2$ batteries, proving the wide applicability of CSE.

4 Conclusions

In this work, we have produced a solid electrolyte with ultra-high ionic conductivity (1.11 mS·cm⁻¹, close to liquid electrolyte) under the premise of ensuring high mechanical properties. The PVDF-HFP-based electrospinning film as support ensures the good mechanical properties of CSE, and the filler is mixed with SN and PVDF-HFP in a ratio of 1:1 as the matrix. The addition of SN greatly reduces the crystallinity of PVDF-HFP, increases the movement of the chain segment, and participates in ion transport, ensuring that CSE has a higher ionic conductivity than most polymer-based solid electrolytes. CSE can also be widely used to assemble stable Li metal, flexible solid-state, Li-O$_2$, and Li-CO$_2$ batteries. This work provides a direction for solving the problem of flexible solid electrolytes with high ionic conductivity and good mechanical properties, and is referenced in the development of safer and more practical flexible solid batteries.

Acknowledgements

Figure 5 (a) Charge–discharge curves of the Li-O$_2$ battery at different current densities with a fixed capacity of 1,000 mAh·g⁻¹. (b) Voltage profiles of the Li-O$_2$ battery at a current density of 400 mA·g⁻¹ with a fixed capacity of 500 mAh·g⁻¹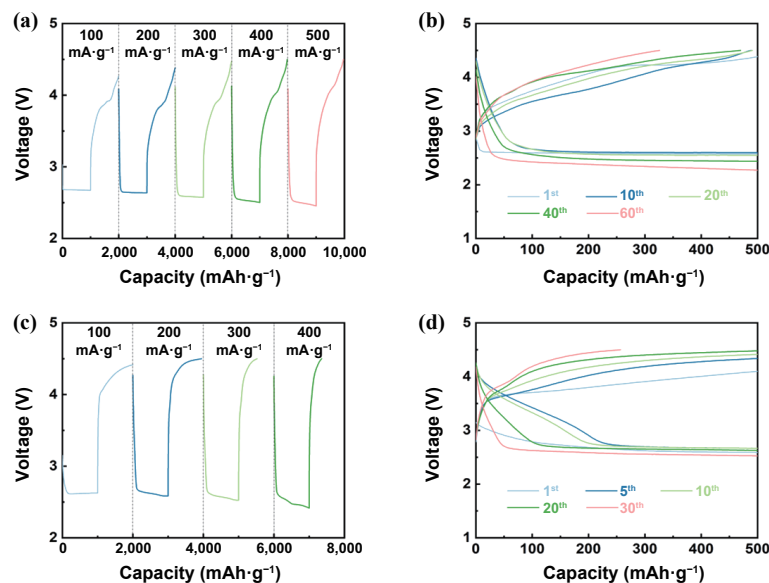. (c) Charge–discharge curves of the Li-CO$_2$ battery at different current densities with a fixed capacity of 1,000 mAh·g⁻¹. (d) Voltage profiles of the Li-CO$_2$ battery at a current density of 200 mA·g⁻¹ with a fixed capacity of 500 mAh·g⁻¹.

Electronic Supplementary Material: Supplementary material (additional material characterizations such as SEM images, photos, XRD and cycle performance of the battery, Nyquist impedance spectra of electrolytes, and Tables on comparisons of the ion conductivity distribution) is available in the online version of this article at https://doi.org/10.1007/s12274-022-4183-z.

References

[1] Dunn, B.; Kamath, H.; Tarascon, J. M. Electrical energy storage for the grid: A battery of choices. *Science* **2011**, *334*, 928–935.

[2] Wang, G.; Xiong, X. H.; Xie, D.; Fu, X. X.; Ma, X. D.; Li, Y. P.; Liu, Y. Z.; Lin, Z.; Yang, C. H.; Liu, M. L. Suppressing dendrite growth by a functional electrolyte additive for robust Li metal anodes. *Energy Storage Mater.* **2019**, *23*, 701–706.

[3] Jena, A.; Meesala, Y.; Hu, S. F.; Chang, H.; Liu, R. S. Ameliorating interfacial ionic transportation in all-solid-state Li-ion batteries with interlayer modifications. *ACS Energy Lett.* **2018**, *3*, 2775–2795.

[4] Wang, C. W.; Fu, K.; Kammampata, S. P.; McOwen, D. W.; Samson, A. J.; Zhang, L.; Hitz, G. T.; Nolan, A. M.; Wachsman, E. D.; Mo, Y. F. et al. Garnet-type solid-state electrolytes: Materials, interfaces, and batteries. *Chem. Rev.* **2020**, *120*, 4257–4300.

[5] He, Z. J.; Fan, L. Z. Poly(ethylene carbonate)-based electrolytes with high concentration Li salt for all-solid-state lithium batteries. *Rare Met.* **2018**, *37*, 488–496.

[6] Shi X. M.; Zeng Z. C.; Sun M. Z.; Huang B. L.; Zhang H. T.; Luo W.; Huang Y. H.; Du Y. P.; Yan C. H. Fast Li-ion conductor of Li_3HoBr_6 for stable all-solid-state lithium-sulfur battery. *Nano Lett.* **2021**, *21*, 9325–9331.

[7] Zou, Z. Y.; Li, Y. J.; Lu, Z. H.; Wang, D.; Cui, Y. H.; Guo, B. K.; Li, Y. J.; Liang, X. M.; Feng, J. W.; Li, H. et al. Mobile ions in composite solids. *Chem. Rev.* **2020**, *120*, 4169–4221.

[8] Zhang, W. Q.; Nie, J. H.; Li, F.; Wang, Z. L.; Sun, C. W. A durable and safe solid-state lithium battery with a hybrid electrolyte membrane. *Nano Energy* **2018**, *45*, 413–419.

[9] Bannister, D. J.; Davies, G. R.; Ward, I. M.; McIntyre, J. E. Ionic conductivities for poly(ethylene oxide) complexes with lithium salts of monobasic and dibasic acids and blends of poly(ethylene oxide) with lithium salts of anionic polymers. *Polymer* **1984**, *25*, 1291–1296.

[10] Sun, X. G.; Kerr, J. B. Synthesis and characterization of network single ion conductors based on comb-branched polyepoxide ethers and lithium bis(allylmalonato)borate. *Macromolecules* **2006**, *39*, 362–372.

[11] Zhang, X.; Liu, T.; Zhang, S. F.; Huang, X.; Xu, B. Q.; Lin, Y. H.; Xu, B.; Li, L. L.; Nan, C. W.; Shen, Y. Synergistic coupling between $Li_{6.75}La_3Zr_{1.75}Ta_{0.25}O_{12}$ and poly(vinylidene fluoride) induces high ionic conductivity, mechanical strength, and thermal stability of solid composite electrolytes. *J. Am. Chem. Soc.* **2017**, *139*, 13779–13785.

[12] Zhai, H. W.; Xu, P. Y.; Ning, M. Q.; Cheng, Q.; Mandal, J.; Yang, Y. A flexible solid composite electrolyte with vertically aligned and connected ion-conducting nanoparticles for lithium batteries. *Nano Lett.* **2017**, *17*, 3182–3187.

[13] Chen, L.; Li, Y. T.; Li, S. P.; Fan, L. Z.; Nan, C. W.; Goodenough, J. B. PEO/garnet composite electrolytes for solid-state lithium batteries: From "ceramic-in-polymer" to "polymer-in-ceramic". *Nano Energy* **2018**, *46*, 176–184.

[14] Das, S.; Ghosh, A. Charge carrier relaxation in different plasticized PEO/PVDF-HFP blend solid polymer electrolytes. *J. Phys. Chem. B* **2017**, *121*, 5422–5432.

[15] Chen, G. H.; Zhang, F.; Zhou, Z. M.; Li, J. R.; Tang, Y. B. A flexible dual-ion battery based on PVDF-HFP-modified gel polymer electrolyte with excellent cycling performance and superior rate capability. *Adv. Energy Mater.* **2018**, *8*, 1801219.

[16] Shi, J.; Yang, Y. F.; Shao, H. X. Co-polymerization and blending based PEO/PMMA/P(VDF-HFP) gel polymer electrolyte for rechargeable lithium metal batteries. *J. Memb. Sci.* **2018**, *547*, 1–10.

[17] Yue, H. Y.; Li, J. X.; Wang, Q. X.; Li, C. B.; Zhang, J.; Li, Q. H.; Li, X. N.; Zhang, H. S.; Yang, S. T. Sandwich-like poly(propylene carbonate)-based electrolyte for ambient-temperature solid-state lithium ion batteries. *ACS Sustainable Chem. Eng.* **2018**, *6*, 268–274.

[18] Li, J.; Lin, Y.; Yao, H. H.; Yuan, C. F.; Liu, J. Tuning thin-film electrolyte for lithium battery by grafting cyclic carbonate and combed poly(ethylene oxide) on polysiloxane. *ChemSusChem* **2014**, *7*, 1901–1908.

[19] Liu, M. Z.; Jin, B. Y.; Zhang, Q. H.; Zhan, X. L.; Chen, F. Q. High-performance solid polymer electrolytes for lithium ion batteries based on sulfobetaine zwitterion and poly (ethylene oxide) modified polysiloxane. *J. Alloys Compd.* **2018**, *742*, 619–628.

[20] Liu, K.; Zhang, Q. Q.; Thapaliya, B. P.; Sun, X. G.; Ding, F.; Liu, X. J.; Zhang, J. L.; Dai, S. *In situ* polymerized succinonitrile-based solid polymer electrolytes for lithium ion batteries. *Solid State Ion.* **2020**, *345*, 115159.

[21] Wang, J.; Huang, G.; Chen, K.; Zhang, X. B. An adjustable-porosity plastic crystal electrolyte enables high-performance all-solid-state lithium-oxygen batteries. *Angew. Chem., Int. Ed.* **2020**, *59*, 9382–9387.

[22] Wei, T.; Zhang, Z. H.; Wang, Z. M.; Zhang, Q.; Ye, Y. S.; Lu, J. H.; Rahman, Z. R.; Zhang, Z. U. Ultrathin solid composite electrolyte based on $Li_{6.4}La_3Zr_{1.4}Ta_{0.6}O_{12}$/PVDF-HFP/LiTFSI/succinonitrile for high-performance solid-state lithium metal batteries. *ACS Appl. Energy Mater.* **2020**, *3*, 9428–9435.

[23] Qiu, G. R.; Sun, C. W. A quasi-solid composite electrolyte with dual salts for dendrite-free lithium metal batteries. *New J. Chem.* **2020**, *44*, 1817–1824.

[24] Yi, Q.; Zhang, W. Q.; Li, S. Q.; Li, X. Y.; Sun, C. W. A durable sodium battery with a flexible $Na_3Zr_2Si_2PO_{12}$-PVDF-HFP composite electrolyte and sodium/carbon cloth anode. *ACS Appl. Mater. Interfaces* **2018**, *10*, 35039–35046.

[25] Zha, W. P.; Chen, F.; Yang, D. J.; Shen, Q.; Zhang, L. M. High-performance $Li_{6.4}La_3Zr_{1.4}Ta_{0.6}O_{12}$/poly(ethylene oxide)/succinonitrile composite electrolyte for solid-state lithium batteries. *J. Power Sources* **2018**, *397*, 87–94.

[26] Alarco, P. J.; Abu-Lebdeh, Y.; Abouimrane, A.; Armand, M. The plastic-crystalline phase of succinonitrile as a universal matrix for solid-state ionic conductors. *Nat. Mater.* **2004**, *3*, 476–481.

[27] Choi, J. H.; Lee, C. H.; Yu, J. H.; Doh, C. H.; Lee, S. M. Enhancement of ionic conductivity of composite membranes for all-solid-state lithium rechargeable batteries incorporating tetragonal $Li_7La_3Zr_2O_{12}$ into a polyethylene oxide matrix. *J. Power Sources* **2015**, *274*, 458–463.

[28] Wang, C.; Zhang, H. R.; Dong, S. M.; Hu, Z. L.; Hu, R. X.; Guo, Z. Y.; Wang, T.; Cui, G. L.; Chen, L. Q. High polymerization conversion and stable high-voltage chemistry underpinning an *in situ* formed solid electrolyte. *Chem. Mater.* **2020**, *32*, 9167–9175.

[29] Xue, Y.; Quesnel, D. J. Synthesis and electrochemical study of sodium ion transport polymer gel electrolytes. *RSC Adv.* **2016**, *6*, 7504–7510.

[30] Kumar, D.; Hashmi, S. A. Ion transport and ion-filler-polymer interaction in poly(methyl methacrylate)-based, sodium ion conducting, gel polymer electrolytes dispersed with silica nanoparticles. *J. Power Sources* **2010**, *195*, 5101–5108.

[31] Zhang, C. H.; Gamble, S.; Ainsworth, D.; Slawin, A. M. Z.; Andreev, Y. G.; Bruce, P. G. Alkali metal crystalline polymer electrolytes. *Nat. Mater.* **2009**, *8*, 580–584.

[32] Liu, M.; Zhou, D.; He, Y. B.; Fu, Y. Z.; Qin, X. Y.; Miao, C.; Du, H. D.; Li, B. H.; Yang, Q. H.; Lin, Z. Q. et al. Novel gel polymer electrolyte for high-performance lithium-sulfur batteries. *Nano Energy* **2016**, *22*, 278–289.

[33] Wong, D. H. C.; Thelen, J. L.; Fu, Y. B.; Devaux, D.; Pandya, A. A.; Battaglia, V. S.; Balsara, N. P.; DeSimone, J. M. Nonflammable perfluoropolyether-based electrolytes for lithium batteries. *Proc. Natl. Acad. Sci. USA* **2014**, *111*, 3327–3331.

[34] Hori, M.; Aoki, Y.; Maeda, S.; Tatsumi, R.; Hayakawa, S. Thermal stability of ionic liquids as an electrolyte for lithium-ion batteries. *ECS Trans.* **2010**, *25*, 147.

[35] Xiao, W.; Li X. H.; Wang Z. X.; Guo H. J.; Wang J. X.; Huang S. L.; Gan L. Physicochemical properties of a novel composite polymer electrolyte doped with vinyltrimethoxylsilane-modified nano-La_2O_3. *J. Rare Earths* **2012**, *30*, 1034–1040.

[36] Oh, S.; Nguyen, V. H.; Bui, V. T.; Nam, S.; Mahato, M.; Oh, I. K. Intertwined nanosponge solid-state polymer electrolyte for rollable and foldable lithium-ion batteries. *ACS Appl. Mater. Interfaces* **2020**, *12*, 11657–11668.

[37] Zhang Q.; Gao Z. Q.; Shi X. M.; Zhang C.; Liu K.; Zhang J.; Zhou L.; Ma C. J.; Du Y. P. Recent advances on rare earths in solid lithium ion conductors. *J. Rare Earths* **2021**, *39*, 1–10.

[38] Rey, I.; Lassègues, J. C.; Grondin, J.; Servant, L. Infrared and Raman study of the PEO-LiTFSI polymer electrolyte. *Electrochim. Acta* **1998**, *43*, 1505–1510.

[39] Zhang, X. L.; Gong, Y. D.; Li, S. Q.; Sun, C. W. Porous perovskite $La_{0.6}Sr_{0.4}Co_{0.8}Mn_{0.2}O_3$ nanofibers loaded with RuO_2 nanosheets as an efficient and durable bifunctional catalyst for rechargeable $Li\text{-}O_2$ batteries. *ACS Catal.* **2017**, *7*, 7737–7747.

[40] Wang, F.; Li, Y.; Xia, X. H.; Cai, W.; Chen, Q. G.; Chen, M. H. Metal–CO_2 electrochemistry: From CO_2 recycling to energy storage. *Adv. Energy Mater.* **2021**, *11*, 2100667.

[41] Shi Q. L.; Zhang H.; Li T. J.; Yu F. L.; Hou H. J.; Han P. D. Preparation and characterization of LSO-SDC composite electrolytes. *J. Rare Earths* **2021**, *33*, 304–309.

[42] Wei W. Q.; Liu B. Q.; Gan Y. Q.; Ma H. J.; Cui D. W. Protecting lithium metal anode in all-solid-state batteries with a composite electrolyte. *Rare Met.* **2021**, *40*, 409–416.